

双数态光的非相位模糊测量

时泽准, 周立坤, 金光日*

浙江理工大学物理学系, 浙江 杭州 310018

摘要 双数态是量子相位估计问题中的有用资源,其作为马赫-曾德尔干涉仪输入态,可使得相位测量精度突破标准量子极限。然而,符合计数探测导致双数态的相位分布函数(即似然函数)出现多峰结构,出现相位模糊。针对这一问题,提出一种可消除相位模糊的简便方案,并对其有效性进行分析。该方案的核心是将 N 光子双数态和单光子分别注入干涉仪中,使得总的相位分布函数具有单峰结构,由此得到唯一最大似然估计量,该估计量的涨落在整个相位区间均优于标准量子极限。

关键词 测量; 量子度量学; 双数态; 相位模糊性; 最大似然估计

中图分类号 O413 **文献标志码** A

DOI: 10.3788/AOS0212006

1 引言

参数或相位估计的核心任务之一就是针对实验测量结果进行数据处理,构造未知参数或相位的估计量。根据经典测量理论,估计量与实际相位的均方根误差取决于独立测量次数以及费舍(Fisher)信息,后者由测量结果的概率密度定义。将量子度量学结合量子力学和统计学基本理论,发现估计精度的最终下限与输入态制备、相位积累方式,以及测量方案等有关。对于多粒子系统的准经典态(例如相干态),相位不确定度与入射态粒子数量 N 的 $1/2$ 次方成反比,因此将其称为标准量子极限(SQL)。对于纠缠态(例如NOON态^[1-2]),相位灵敏度与 N 成反比,因此将其称为海森堡极限(HL)。与标准量子极限相比,海森堡极限的相位估计精度提高了 \sqrt{N} 倍。在过去的几十年里,该领域吸引了大量的关注,引力波探测^[3-4]、生物传感^[5-6]、原子钟^[7-8]等也展现出良好的发展前景。

纠缠NOON态的量子费舍信息正比于 N^2 ,因此其估计精度的下限——克拉美罗界与 N 成反比,达到海森堡极限。然而,该态在实验中难以制备,并且易受环境影响而损耗^[1]。相对于NOON态,双数态对环境更具鲁棒性^[9-10],其量子费舍信息等于 $N(N+2)/2$,虽然略低于NOON态的量子费舍信息,但是其相位测量精度依然可达海森堡标度。2013年,Xiang等^[11-12]通过实验演示了6光子双数态的制备,并从理论上提出:对于所谓的单条纹探测,双数态的费舍信息反而优于NOON态。这里采用的单条纹探测其实是一个双输

出结果测量^[13],即在干涉仪两个输出端口进行符合计数测量,将其中光子数量 $n_1 = n_2 = N/2$ 作为一种测量结果(outcome),并将其他光子探测事件统一视为另一种测量结果。这种双输出测量在量子信息的其他领域也普遍使用,例如根据探测光子数量的奇偶性进行判断的宇称测量^[14-15]、on-off测量等领域。

对于多输出测量,相位估计精度还取决于测量方案和数据处理。目前实验上普遍采用基于平均输出信号的反函数估计量,该估计量的测量精度由误差传递公式度量^[16]。双数态马赫-曾德尔干涉仪对光强差的测量失效,这是因为输出信号始终为0,对相位变化无响应,无法得到相位的反函数估计量。为了解决这个问题,人们提出单条纹探测^[11-12]和宇称测量^[14-15],以及 \hat{J}_z^2 测量^[17-18]等方法。2019年,Xu等^[19]将最大似然估计量用于双数态的光强差测量实验,然而这种数据处理方法存在一个问题——相位模糊性。具体来说,由于双数态测值概率具有周期性,最大似然函数在一个相位周期内存在多峰结构,例如,Xu等^[19]通过数值研究发现最大似然函数在 $\theta \in (-\pi, \pi)$ 区间出现4个峰,因此无法确定哪一个峰值位置与相位真值接近。相位模糊性在NOON态情况下也会出现,其解决方案主要是联合不同周期的态进行测量,如使用多种NOON态^[20]、NOON态的反馈相位^[21],以及单光子与NOON态的反馈相位^[22]等方法。

针对双数态在马赫-曾德尔干涉仪的光强差测量方面存在的问题,本文提出一种消除相位模糊的方案,并对其有效性给出分析。所提方案分4步:第一步,采

收稿日期: 2022-06-06; 修回日期: 2022-07-14; 录用日期: 2022-07-25; 网络首发日期: 2022-08-05

基金项目: 国家自然科学基金(12075209)、浙江理工大学科学基金(18062145-Y)

通信作者: *grjin@zstu.edu.cn

取与 Xu 等^[19]完全相同的相位估计方案,即在干涉仪中不添加偏置相位,统计每个输出结果的出现次数,得出不加偏置相位测量的似然函数;第二步,在干涉仪中添加一个偏置相位,重复不加偏置相位的步骤,得出添加偏置相位测量的似然函数,然后将其与第一步中的似然函数相乘,得到联合测量的似然函数;第三步,注入单光子态,并在干涉仪中设置一个偏置相位,它由第二步中联合似然函数的最大值位置确定;第四步,将上述 3 个步骤得到的相位分布函数相乘,得到一个单峰结构的似然函数,用于唯一地确定最大似然估计量。

2 双数态在马赫-曾德尔干涉仪中的符合计数测量

在描述测量过程之前,首先给出马赫-曾德尔干涉仪的数学描述。如图 1 所示,马赫-曾德尔干涉仪通常由两个 50:50 分束器和一个相移器组成,借助于双模玻色算符的 Schwinger 表示,马赫-曾德尔干涉仪可用如下么正算符^[23]描述为

$$U_{MZI}(\phi) = \exp(-i\pi J_x/2) \exp(i\phi J_z) \exp(i\pi J_x/2) = \exp(-i\phi J_y), \quad (1)$$

式中: ϕ 为相位; J_x, J_y, J_z 为角动量算符,由泡利矩阵 $\sigma_i (i=x, y, z)$ 定义。

$$J_i = \frac{1}{2} (a_1^\dagger, a_2^\dagger) \sigma_i \begin{pmatrix} a_1 \\ a_2 \end{pmatrix}, \quad (2)$$

式中: $a_1, a_1^\dagger, a_2, a_2^\dagger$ 为两个模式的产生和湮灭算符。

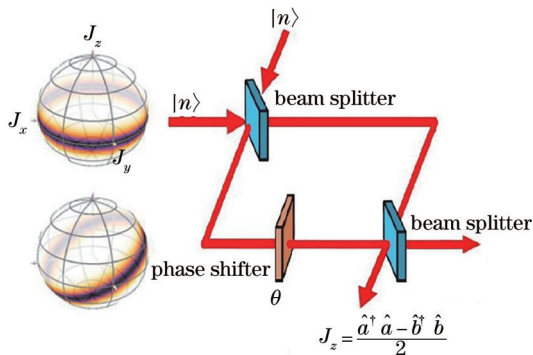


图 1 马赫-曾德尔干涉仪中双数态光源测量示意图

Fig. 1 Schematic of measurement using twin-Fock states of light source in Mach-Zehnder interferometer

Holland 和 Burnett^[24]最早提出用双数态作为马赫-曾德尔干涉仪的输入态,实现对未知相位 ϕ 的估计,即 $|n_1\rangle \otimes |n_2\rangle$,下角标表示光场的两个正交模式,例如马赫-曾德尔干涉仪的两个光路,或者偏振马赫-曾德尔干涉仪的横向或纵向偏振模式。对于任一双模数态 $|n_1\rangle \otimes |n_2\rangle$,可用 J_z 算符的本征态 $|j, k\rangle$ 重新表示,其中 $j = (n_1 + n_2)/2 = N/2$ 为总角动量数, $k = (n_1 - n_2)/2$ 为赝自旋的磁角动量数。作为特例,双数态 $|n\rangle \otimes |n\rangle = |j, 0\rangle$ 。

根据双数态马赫-曾德尔干涉仪的光强差测量,得到的测值概率为

$$P_k(\theta) = \left| \langle j, k | \exp(-i\theta J_y) | j, 0 \rangle \right|^2 = \left[d_{k,0}^{(j)}(\theta) \right]^2, \quad (3)$$

式中: $d_{k,l}^{(j)}(\theta) = \langle j, k | \exp(-i\theta J_y) | j, l \rangle$ 为 Wigner's d 矩阵^[25]。根据经典度量学理论,相位测量精度的下限由克拉美罗界^[26]决定,即

$$\delta\theta \geq \delta\theta_{\text{CRB}} = \frac{1}{\sqrt{\mathcal{N}F(\theta)}}, \quad (4)$$

式中: \mathcal{N} 为测量的次数或者数据集的大小; $F(\theta)$ 为经典费舍信息^[27],可表示为

$$\begin{cases} F(\theta) = \sum_k f_k(\theta) \\ f_k(\theta) = \frac{1}{P_k(\theta)} \left[\frac{\partial P_k(\theta)}{\partial \theta} \right]^2 \end{cases} \quad (5)$$

在实际情况下,由于实验存在缺陷(如存在噪声、光子损耗^[9,20]),克拉美罗界一般不能达到。为了模拟实验缺陷,对各输出概率做如下修正(本文的实验模拟采用文献^[19]的模型),即

$$P_k^{\text{im}}(\theta) = A_0 P_k(\theta) + B_k, k = 0, 1, 2, 3, \quad (6)$$

式中: $A_0 = 0.9293; B_0 = 0.0245; B_1 = 0.0087; B_2 = 0.0068; B_3 = 0.0076$;上标 im 表示它是假想的概率。修正后的概率函数同样满足“相反本征值的概率函数相同,概率函数总和等于 1”的要求。

对于单光子态 $|1\rangle \otimes |0\rangle$ 和 $|0\rangle \otimes |1\rangle$,也可以将角动量态写成 $|j = 1/2, k = \pm 1/2\rangle$,则测值概率函数^[20]为

$$\begin{cases} P_{1/2}(\theta) = \left[d_{1/2,1/2}^{(1/2)}(\theta) \right]^2 = \cos^2\left(\frac{\theta}{2}\right) \\ P_{-1/2}(\theta) = 1 - P_{1/2}(\theta) \end{cases} \quad (7)$$

将式(7)代入式(5),可得单个光子的费舍信息等子于 1,因此相位测量精度下限 $\delta\theta_{\text{CRB}} = 1/\sqrt{\mathcal{N}^{(S)}}$ 可达到标准量子极限,其中 $\mathcal{N}^{(S)}$ 为单光子测量次数。类似地,对单光子概率进行修正^[13]: $P_{1/2}^{\text{im}}(\theta) = aP_{1/2}(\theta) + b$ 和 $P_{-1/2}^{\text{im}}(\theta) = 1 - P_{1/2}^{\text{im}}(\theta)$,其中, $a = 0.98800, b = 0.00396$ 。

对修正概率进行蒙特卡罗模拟,结果如图 2 所示。对每个采样点 θ 使用 500 个随机数并记录每个输出结果出现的频率 $\mathcal{N}_k/\mathcal{N}$,然后重复 20 次得到平均值(实线附近的点)和方差(误差棒),各输出概率便可由频率的统计平均值拟合得到(实线)。对于双数态,对施加了偏置相位的干涉仪重复上述步骤,结果如图 2(a)~(d)的虚线所示。

3 相位模糊性问题及消除策略

3.1 有限离散输出下的最大似然估计与似然函数的近似

第 2 节给出了马赫-曾德尔干涉仪中双数态光源

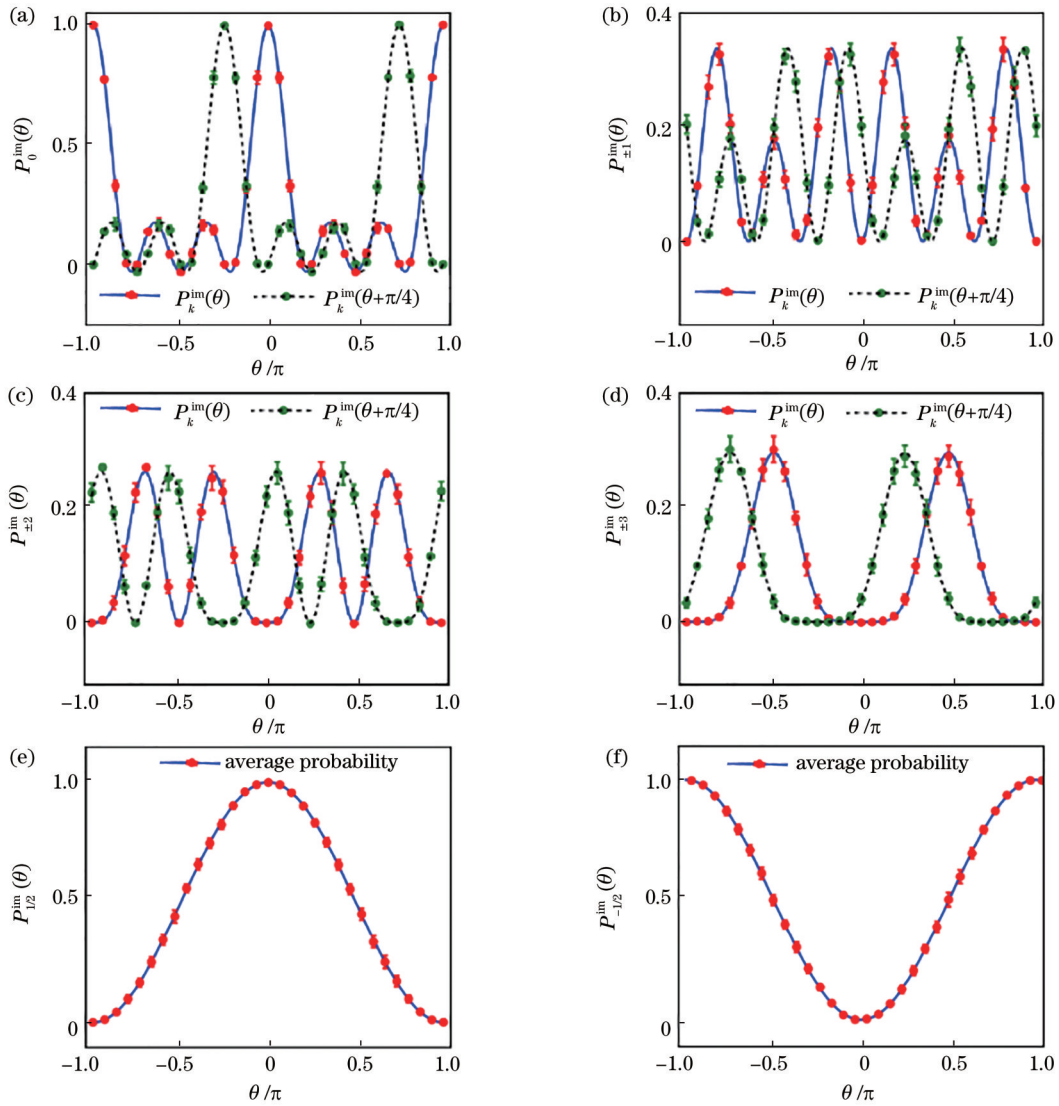


图 2 双数态和单光子态粒子数差探测结果概率模拟。(a)六光子双数态 $k=0$; (b)六光子双数态 $k=\pm 1$; (c)六光子双数态 $k=\pm 2$; (d)六光子双数态 $k=\pm 3$; (e)单光子态 $k=1/2$; (f)单光子态 $k=-1/2$

Fig. 2 Probability simulation of the difference in the number of particles in twin-Fock state and single-photon state. (a) Six-photon twin-Fock state with $k=0$; (b) six-photon twin-Fock state with $k=\pm 1$; (c) six-photon twin-Fock state with $k=\pm 2$; (d) six-photon twin-Fock state with $k=\pm 3$; (e) single-photon state with $k=1/2$; (f) single-photon state with $k=-1/2$

粒子数差测量的概率函数。根据经典度量学理论,可以通过观测结果和测值概率函数获得对未知参数的估计。最常用的估计方法之一是最大似然估计,即计算似然函数后取似然函数的最大值点。本文引出有限离散输出下最大似然估计的一般形式,并推导它的近似解析结果。

似然函数与概率函数的形式相同,区别在于似然函数的相位真值为变量,观测数据为已知量。对于多个独立观测数据,它们的联合概率函数为单一概率函数的乘积。一般地,当观测变量离散且可能取值有限时,很显然概率函数(似然函数)取以下形式

$$\mathcal{P}(\theta|\{\mathcal{N}_\mu\}) \propto \prod_{\mu} [P_{\mu}(\theta)]^{\mathcal{N}_{\mu}}, \quad (8)$$

式中: μ 为观测变量; $P_{\mu}(\theta)$ 表示测量结果为 μ 的函数;

\mathcal{N}_{μ} 为对观测结果 μ 的测量次数,总测量次数 $\mathcal{N} = \sum_{\mu} \mathcal{N}_{\mu}$ 。为了区分双数态和单光子态,使用 $\{\mathcal{N}_{\mu}^{(T)}\}$ 标记双数态的测量结果,其总测量次数为 $\mathcal{N}^{(T)} = \sum_{\mu=-j}^j \mathcal{N}_{\mu}^{(T)}$;使用 $\{\mathcal{N}_{\mu}^{(S)}\}$ 标记单光子态的测量结果,其总测量次数 $\mathcal{N}^{(S)} = \mathcal{N}_{1/2}^{(S)} + \mathcal{N}_{-1/2}^{(S)}$ 。

文献[28]中给出了 \mathcal{N} 趋于无穷大时式(8)在似然函数最大值位置附近的近似形式:对于每一个观测结果 μ ,反函数估计量 $\theta_{inv,\mu}$ 的定义式为 $P_{\mu}(\theta_{inv,\mu}) = \mathcal{N}_{\mu}/\mathcal{N}$ 。显然 \mathcal{N} 趋于无穷大时, $\theta_{inv,\mu}$ 接近似然函数最大值的位置,于是可以对 $P_{\mu}(\theta)$ 在 $\theta_{inv,\mu}$ 使用一阶泰勒展开,得到

$$P_{\mu}(\theta) \approx P_{\mu}(\theta_{\text{inv},\mu}) \left[1 + \frac{P'_{\mu}(\theta_{\text{inv},\mu})}{P_{\mu}(\theta_{\text{inv},\mu})} (\theta - \theta_{\text{inv},\mu}) \right], \quad (9)$$

式中: $P'_{\mu}(\theta_{\text{inv},\mu})$ 为 $P_{\mu}(\theta)$ 在 $\theta_{\text{inv},\mu}$ 处的一阶导数。

对式(9)使用泰勒近似公式 $(1+x)^n \approx \exp[nx(1-x/2)]$ 展开, 有:

$$[P_{\mu}(\theta)]^{\mathcal{N}_{\mu}} \approx P_{\mu}(\theta_{\text{inv},\mu})^{\mathcal{N}_{\mu}} \exp \left\{ \frac{\mathcal{N}_{\mu}}{2} \frac{P'_{\mu}(\theta_{\text{inv},\mu})}{P_{\mu}(\theta_{\text{inv},\mu})} (\theta - \theta_{\text{inv},\mu}) \left[1 - \frac{P'_{\mu}(\theta_{\text{inv},\mu})}{P_{\mu}(\theta_{\text{inv},\mu})} (\theta - \theta_{\text{inv},\mu}) \right] \right\}. \quad (10)$$

将式(10)代入式(8), 注意到 $\sum_{\mu} P'_{\mu} = 0$, 整理得:

$$\begin{aligned} \mathcal{P}(\theta|\{\mathcal{N}_{\mu}\}) &\propto \prod_{\mu} P_{\mu}(\theta_{\text{inv},\mu})^{\mathcal{N}_{\mu}} \times \\ &\exp \left[-\frac{\mathcal{N}}{2} \sum_{\mu} \frac{P'_{\mu}(\theta_{\text{inv},\mu})}{P_{\mu}(\theta_{\text{inv},\mu})} \theta_{\text{inv},\mu} \right] \times \\ &\exp \left[-\frac{\mathcal{N}}{2} \sum_{\mu} \frac{P_{\mu}'^2(\theta_{\text{inv},\mu})}{P_{\mu}(\theta_{\text{inv},\mu})} (\theta - \theta_{\text{inv},\mu})^2 \right]. \end{aligned} \quad (11)$$

忽略式(11)等号右边的前两个常数项, 有

$$\mathcal{P}(\theta|\{\mathcal{N}_{\mu}\}) \Big|_{\theta \rightarrow \theta_0} \propto \exp \left[-\frac{1}{2\sigma_{\text{est}}^2} (\theta - \theta_{\text{est}})^2 \right], \quad (12)$$

式中: σ_{est}^2 为方差; θ_{est} 为相位估计量。

$$\begin{cases} \theta_{\text{est}} = \sum_{\mu} c_{\mu} \theta_{\text{inv},\mu} \\ c_{\mu} = f_{\mu}(\theta_{\text{inv},\mu}) / \sum_{\mu'} f_{\mu'}(\theta_{\text{inv},\mu'}) \end{cases}, \quad (13)$$

式中: $f_{\mu}(\theta_{\text{inv},\mu})$ 为式(5)定义的第 μ 个观测量在 $\theta_{\text{inv},\mu}$ 处的费舍信息。方差可表示为

$$\sigma_{\text{est}}^2 = \left[\mathcal{N} \sum_{\mu} f_{\mu}(\theta_{\text{inv},\mu}) \right]^{-1}. \quad (14)$$

3.2 相位模糊性消除策略及估计量的统计性能分析

根据经典度量学理论, 最大似然估计是一种渐进无偏的有效估计。也就是, 当测量次数足够大时, 最大似然估计量的统计平均值接近真值, 统计方差接近克拉美罗界。然而, 双数态光源的相位分布函数具有多峰结构, 在一个相位周期内无法确定唯一的最大似然估计量, 由此导致了相位模糊性问题。针对这个问题, 提出一种消除相位模糊的方案并给出数值模拟结果, 同时将给出方案的有效性以及估计量统计性能的分析。

本实验的测量策略如下: 第一步, 发射 $\mathcal{N}^{(T)}$ 组双数态不加偏置相位, 统计每个输出结果 k 的测量次数 $\mathcal{N}_k^{(T)}$, 获得似然函数 $\mathcal{P}(\theta|\{\mathcal{N}_k^{(T)}\})$ 。图 3(a) 所示为 100 组六光子双数态无偏置相位的测量结果, 取相位真值 $\theta_0 = 0.4\pi$, 输入态为六光子双数态, 总输入组数 $\mathcal{N}^{(T)} = 100$ 。可以看到, 在区间 $(-\pi, \pi)$ 上似然函数出现了 4 个最大值点。第二步, 在干涉仪中添加一个偏置相位 $\varphi = \pi/4$, 并发射 $\mathcal{M}^{(T)} = 10$ 组双数态, 得出添

加偏置相位后的似然函数 $\mathcal{P}(\theta + \varphi|\{\mathcal{M}_k^{(T)}\})$ 。在图 3(b) 中, 虚线为添加偏置相位时测量的数值结果。可以明显观察到, 相对于不加偏置相位时测量的似然函数, 添加偏置相位时测量的似然函数有两个最大值点的位置发生了变化, 从而使联合测量的似然函数 $\mathcal{P}(\theta|\{\mathcal{N}_k^{(T)}\})(\theta + \varphi|\{\mathcal{M}_k^{(T)}\})$ 只有两个最大值点(图 3 虚线和实线重合部分)。第三步, 发射单光子态^[29], 并在干涉仪中设置一个偏置相位 ϕ , 其值等于第二步中联合似然函数在 $(0, \pi)$ 上的最大值位置的相反数。根据测量结果, 获得单光子的似然函数 $\mathcal{P}(\theta - \phi|\{\mathcal{N}_k^{(S)}\})$ 。图 3(c) 给出了单光子测量的数值模拟结果, 单光子态的输入个数为 $\mathcal{N}^{(S)} = 10$ 。可以看到, 单光子的似然函数集中在 ϕ 附近, 而在 $\phi - \pi$ 附近的函数值接近于 0。需要注意的是, 虽然在图 3(c) 中单光子的似然函数呈单峰结构, 但这种情况只在单光子仅在一个端口被检测到时发生, 其概率为 $[P_{1/2}(\theta_0 - \phi)]^{\mathcal{N}^{(S)}}$; 而在其他情况下, 单光子似然函数将有两个峰, 位于 $\phi \pm 2\sqrt{\arccos[\mathcal{N}_{1/2}^{(S)}/\mathcal{N}^{(S)}]}$ 处。

在完成以上三步测量后, 得到总的相位分布函数:

$$\mathcal{P}(\theta) = (\theta|\{\mathcal{N}_k^{(T)}\})(\theta + \varphi|\{\mathcal{M}_k^{(T)}\})(\theta - \phi|\{\mathcal{N}_k^{(S)}\}). \quad (15)$$

而本实验的估计量即为 $\mathcal{P}(\theta)$ 在区间 $(-\pi, \pi)$ 内的最大值点, 可通过数值方法计算。图 3 显示了消除相位模糊性策略中的似然函数。其中, 图 3(d) 所示为式(15)的数值模拟结果, 可以看到其在该区间内只有一个峰, 消除了相位模糊。

实施所提方案的关键在于添加偏置相位时似然函数的两个最大值点的位置发生了变化, 接下来证明这个位置的变化量约为 -2φ 。由于 $P_k(\pi - \theta) = P_k(\theta) = \mathcal{N}_k^{(T)}/\mathcal{N}^{(T)}$, 因此反函数估计量并不是唯一的, 将其标记为真值附近的解 $\theta_{\text{inv},k}^{(1)} = P_k^{-1}[\mathcal{N}_k^{(T)}/\mathcal{N}^{(T)}]$, 于是获得另一个反函数估计量 $\theta_{\text{inv},k}^{(2)} = \pi - P_k^{-1}[\mathcal{N}_k^{(T)}/\mathcal{N}^{(T)}] = \pi - \theta_{\text{inv},k}^{(1)}$ 。将 $\theta_{\text{inv},k}^{(1)}$ 和 $\theta_{\text{inv},k}^{(2)}$ 分别代入式(13), 可以得到似然函数的最大值位置 $\theta_{\text{est}}^{(1)} = \sum_k c_k \theta_{\text{inv},k}^{(1)}$ 和 $\theta_{\text{est}}^{(2)} = \pi - \theta_{\text{est}}^{(1)}$ 。

由 $P_k(\pi - \varphi - \theta) = P_k(\theta + \varphi) = \mathcal{M}_k^{(T)}/\mathcal{M}^{(T)}$ 可以得到添加偏置相位后的估计量 $\theta_{\text{inv},k}^{(1)} = P_k^{-1}[\mathcal{M}_k^{(T)}/\mathcal{M}^{(T)}] - \varphi$ 和 $\theta_{\text{inv},k}^{(2)} = \pi - \varphi - P_k^{-1}[\mathcal{M}_k^{(T)}/\mathcal{M}^{(T)}] = \pi - 2\varphi - \theta_{\text{inv},k}^{(1)}$ 。同理, 似然函数的最大值位置近似为 $\theta_{\text{est}}^{(1)} = \sum_k c_k \theta_{\text{inv},k}^{(1)}$ 和 $\theta_{\text{est}}^{(2)} = \pi - 2\varphi - \theta_{\text{est}}^{(1)}$ 。也就是说, 添加偏置相位后 $\theta_{\text{est}}^{(2)}$ 对应的位置减少了 2φ 。在本次数值模拟中, 施加偏置相位前后 $\theta_{\text{est}}^{(2)}$ 的位置距离要尽可能远, 且相位周期等于 π , 因此选取 $2\varphi = \pi/2$ 。

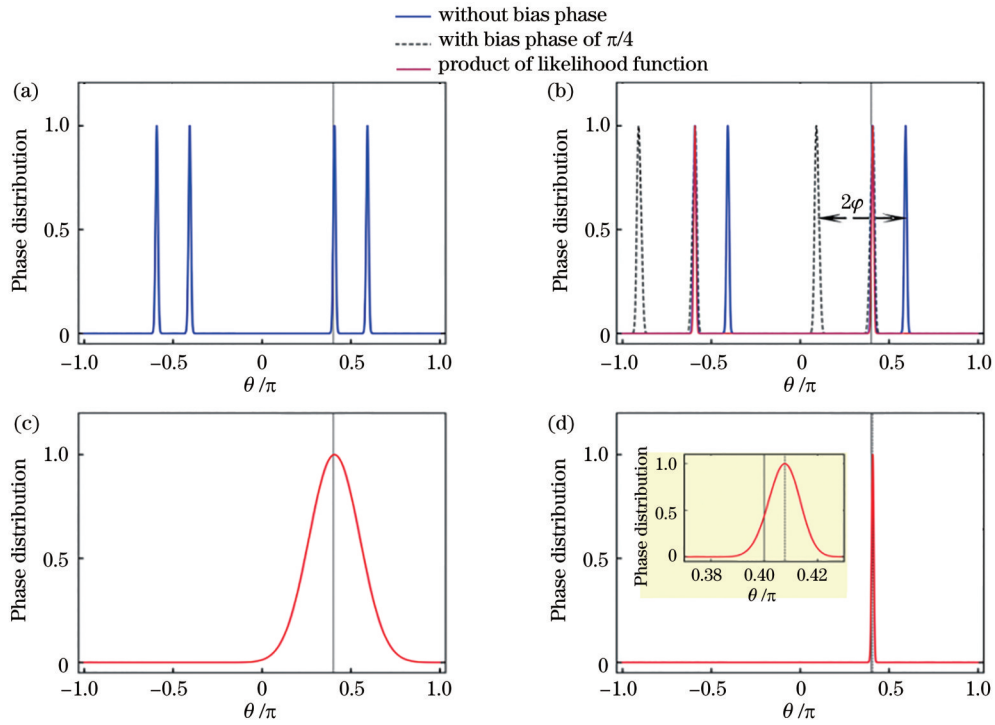


图 3 消除相位模糊性策略中的似然函数。(a) 100 组无偏置相位的六光子双数态理想测量结果;(b) 100 组无偏置相位和 10 组偏置相位为 $\pi/4$ 的六光子双数态理想测量结果及似然函数的乘积;(c) 10 组单光子态的理想测量结果;(d) 单光子态和双数态似然函数的乘积

Fig. 3 Likelihood function of a simulation to eliminate phase ambiguity. (a) Ideal measurement result of 100 six-photon twin-Fock states without bias phase; (b) ideal measurement results of 100 six-photon twin-Fock states without bias phase and 10 six-photon twin-Fock states with bias phase of $\pi/4$ and product of their likelihood function; (c) ideal measurement result of 10 single-photon state; (d) product of likelihood function of single-photon state and twin-Fock state

最后,评估这个估计量的统计性能。使用修正概率方法获得模拟的测量结果数据,然后通过式(15)获得单次实验模拟的估计量。其中,对于每个相位采样点,使用添加和不加偏置相位的双数态测量组数 $\mathcal{N}^{(T)} = \mathcal{M}^{(T)} = 2000$,单光子态测量组数 $\mathcal{N}^{(S)} = 200$ 。重复这个过程 50 次,得出这个相位采样点的统计测量数据,结果如图 4 所示,其中图 4(a)的点为统计测量数据的约化标准差,即为了消除式(4)中态的输入组数的

经典影响,将模拟实验的标准差乘以 $\sqrt{\mathcal{N}}$,其中 $\mathcal{N} = \mathcal{N}^{(T)} + \mathcal{M}^{(T)} + \mathcal{N}^{(S)}$ 。标记 $F_T(\theta)$ 和 $F_S(\theta)$ 分别为双数态和单光子态的费舍信息,理论上可计算得到约化灵敏度^[13]的下限:

$$\delta\theta \geq \sqrt{\frac{\mathcal{N}^{(T)} + \mathcal{M}^{(T)} + \mathcal{N}^{(S)}}{\mathcal{N}^{(T)}F_T(\theta) + \mathcal{M}^{(T)}F_T(\theta + \varphi) + \mathcal{N}^{(S)}F_S(\theta + \phi)}} \quad (16)$$

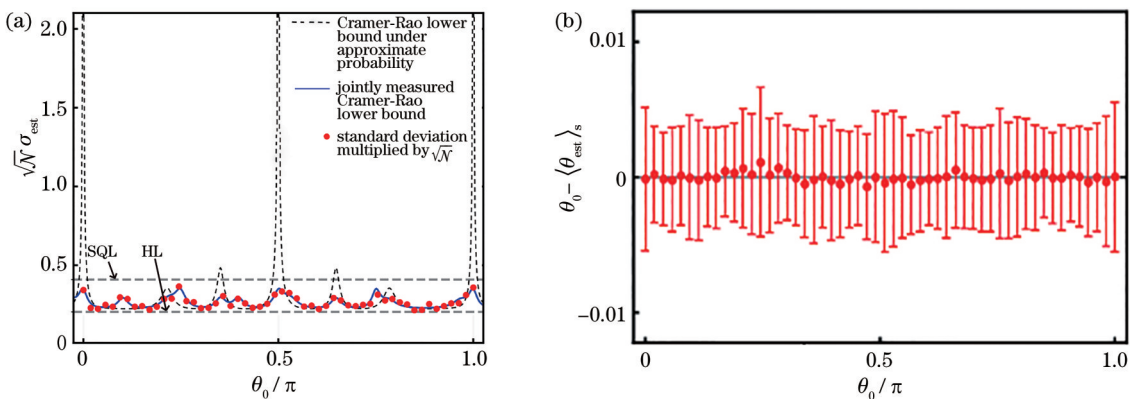


图 4 相位灵敏度随相位的变化关系及测量偏差。(a) 相位灵敏度随相位的变化关系;(b) 估计值与真值的偏差

Fig. 4 Phase sensitivity changed with phase and measurement deviation. (a) Relationship of phase sensitivity and phase; (b) deviation of estimated value from true value

图 4(a)为相位灵敏度随相位的变化图,其中黑色虚曲线为实验近似概率下无偏置相位测量的克拉美罗界^[19],实线为联合测量的克拉美罗界,由式(16)给出。可见本文描述的估计量在全相位区间优于 SQL。将测量标准差与 SQL^[30](图 4 上方水平虚线)及 HL(图 4 下方水平虚线)进行比较,可以看到在 $(0, \pi)$ 区间所测量的相位灵敏度均优于 SQL。图 4(b)所示为估计量与相位真值的偏差,可以看到,在全区间上本文的估计量都是无偏的。

另外,单光子费舍信息对约化灵敏度的贡献很小,可以对估计量进行简化:当 $\mathcal{N}_{1/2}^{(s)} > \mathcal{N}^{(s)}/2$ 时,取 ϕ 为估计量;反之,取 $\phi - \pi$ 为估计量。对于利用所提方法得出的估计量涨落,本文没有展开讨论。

4 结 论

针对双数态粒子数测量的相位模糊问题,提出一种可消除相位模糊的简便实验方案。首先,将偏置相位最大似然估计由双输出推广到多输出,通过给出似然函数的具体图像,发现其可以将相位周期内的 4 个最大值点减少到 2 个。然后,结合多输出似然函数的高斯近似形式给出了这种现象的半解析分析。引入了单光子态的测量,其概率函数的周期为 π ,提供了消除相位模糊的可能。联合这两种态的似然函数得出最终的估计量。最后,对相位估计过程进行数值模拟,发现所得估计量在整个相位区间内的相位灵敏度均优于 SQL。

参 考 文 献

- [1] Mitchell M W, Lundeen J S, Steinberg A M. Super-resolving phase measurements with a multiphoton entangled state[J]. *Nature*, 2004, 429(6988): 161-164.
- [2] Dowling J P. Quantum optical metrology-the lowdown on high-NOON states[J]. *Contemporary Physics*, 2008, 49(2): 125-143.
- [3] Abadie J, Abbott B P, Abbott R, et al. A gravitational wave observatory operating beyond the quantum shot-noise limit[J]. *Nature Physics*, 2011, 7(12): 962-965.
- [4] Aasi J, Abadie J, Abbott B P, et al. Enhanced sensitivity of the LIGO gravitational wave detector by using squeezed states of light[J]. *Nature Photonics*, 2013, 7(8): 613-619.
- [5] Taylor M A, Bowen W P. Quantum metrology and its application in biology[J]. *Physics Reports*, 2016, 615: 1-59.
- [6] Mauranyapin N P, Madsen L S, Taylor M A, et al. Evanescent single-molecule biosensing with quantum-limited precision[J]. *Nature Photonics*, 2017, 11(8): 477-481.
- [7] Ludlow A D, Boyd M M, Ye J, et al. Optical atomic clocks[J]. *Reviews of Modern Physics*, 2015, 87(2): 637-701.
- [8] Katori H. Optical lattice clocks and quantum metrology[J]. *Nature Photonics*, 2011, 5(4): 203-210.
- [9] Dorner U, Demkowicz-Dobrzanski R, Smith B J, et al. Optimal quantum phase estimation[J]. *Physical Review Letters*, 2009, 102(4): 040403.
- [10] Zhang Z, Duan L M. Quantum metrology with Dicke squeezed states[J]. *New Journal of Physics*, 2014, 16(10): 103037.
- [11] Xiang G Y, Hofmann H F, Pryde G J. Optimal multi-photon phase sensing with a single interference fringe[J]. *Scientific Reports*, 2013, 3: 2684.
- [12] Sun F W, Liu B H, Gong Y X, et al. Experimental demonstration of phase measurement precision beating standard quantum limit by projection measurement[J]. *Europhysics Letters*, 2008, 82(2): 24001.
- [13] Jin G R, Yang W, Sun C P. Quantum-enhanced microscopy with binary-outcome photon[J]. *Physical Review A*, 2017, 95(1): 013835.
- [14] Bollinger J J, Itano W M, Wineland D J, et al. Optimal frequency measurements with maximally correlated states[J]. *Physical Review A*, 1996, 54(6): R4649-R4652.
- [15] Gerry C C. Heisenberg-limit interferometry with four-wave mixers operating in a nonlinear regime[J]. *Physical Review A*, 2000, 61(4): 043811.
- [16] Israel Y, Rosen S, Silberberg Y. Supersensitive polarization microscopy using NOON states of light[J]. *Physical Review Letters*, 2014, 112(10): 103604.
- [17] Lücke B, Scherer M, Kruse J, et al. Twin matter waves for interferometry beyond the classical limit[J]. *Science*, 2011, 334(6057): 773-776.
- [18] Kim T, Pfister O, Holland M J, et al. Influence of decorrelation on Heisenberg-limited interferometry with quantum correlated photons[J]. *Physical Review A*, 1998, 57(5): 4004-4013.
- [19] Xu J H, Wang J Z, Chen A X, et al. Optimal phase estimation with photon-number difference measurement using twin-Fock states of light[J]. *Chinese Physics B*, 2019, 28(12): 120303.
- [20] Pezzé L, Smerzi A. Sub shot-noise interferometric phase sensitivity with beryllium ions Schrödinger cat states[J]. *Europhysics Letters*, 2007, 78(3): 30004.
- [21] Xiang G Y, Higgins B L, Berry D W, et al. Entanglement-enhanced measurement of a completely unknown optical phase [J]. *Nature Photonics*, 2011, 5(1): 43-47.
- [22] Gkortsilas N, Cooper J J, Dunningham J A. Measuring a completely unknown phase with sub-shot-noise precision in the presence of loss[J]. *Physical Review A*, 2012, 85(6): 063827.
- [23] Yurke B, McCall S L, Klauder J R. SU(2) and SU(1, 1) interferometers[J]. *Physical Review A*, 1986, 33(6): 4033-4054.
- [24] Holland M J, Burnett K. Interferometric detection of optical phase shifts at the Heisenberg limit[J]. *Physical Review Letters*, 1993, 71(9): 1355-1358.
- [25] Feng X M, Wang P, Yang W, et al. High-precision evaluation of Wigner's d matrix by exact diagonalization[J]. *Physical Review E*, 2015, 92(4): 043307.
- [26] Helstrom C W. Quantum detection and estimation theory[J]. *Journal of Statistical Physics*, 1969, 1(2): 231-252.
- [27] Giovannetti V, Lloyd S, Maccone L. Quantum-enhanced measurements: beating the standard quantum limit[J]. *Science*, 2004, 306(5700): 1330-1336.
- [28] 黄汛, 倪明, 季阳, 等. 光子非全同和光子损失的玻色采样模拟研究[J]. *光学学报*, 2021, 41(12): 1227001.
Huang X, Ni M, Ji Y, et al. Simulation on boson sampling with photon partial distinguishability and photon losses[J]. *Acta Optica Sinica*, 2021, 41(12): 1227001.
- [29] 赵雨辰, 赵博洋, 郑家欢, 等. 具有 3~5 μm 宽带光吸收特性的超导纳米线单光子探测器设计[J]. *激光与光电子学进展*, 2022, 59(1): 0104001.
Zhao Y C, Zhao B Y, Zheng J H, et al. Design of superconducting nanowire single-photon detector with broadband light absorption characteristics in 3-5 μm [J]. *Laser & Optoelectronics Progress*, 2022, 59(1): 0104001.
- [30] Zou Y Q, Wu L N, Liu Q, et al. Beating the classical precision limit with spin-1 Dicke states of more than 10000 atoms[J]. *Proceedings of the National Academy of Sciences of the United States of America*, 2018, 115(25): 6381-6385.

Unambiguous Phase Measurement for Twin-Fock States

Shi Zezhun, Zhou Likun, Jin Guangri*

Physics Department of Zhejiang Sci-Tech University, Hangzhou 310018, Zhejiang, China

Abstract

Objective Metrics play a central role in science and engineering. It is concerned with the final reachable accuracy of parameters or phase estimation and the construction of measurement schemes to achieve this accuracy. By combining quantum mechanics and basic theories of statistics, quantum metrics find that the final lower limit of estimation accuracy is related to input state preparation, phase accumulation modes, and measurement schemes, and the main goal is to break through the standard quantum limit and reach the Heisenberg limit of measurement accuracy. In recent years, due to the progress of experimental conditions, quantum metrics have been widely used in the frontier fields such as gravitational wave detection and atomic clocks. A major research direction of quantum metrics is phase estimation in optical interferometers, which was first proposed in research on the input coherent light and compressed light in Mach-Zende interferometers by Caves *et al.*, and its theoretical phase sensitivity can reach the physical limit (Heisenberg limit). In recent years, other kinds of non-classical light sources have also been studied, such as the NOON state and twin-Fock state. The NOON state is a numerical light source that can theoretically reach the Heisenberg limit, while the twin-Fock state has theoretical phase sensitivity up to the Heisenberg scale and is more robust to photon loss than the NOON state. However, coincidence count detection for the twin-Fock state results in a multi-peak structure of the phase distribution (i. e., the likelihood function), which is the so-called phase ambiguity. Aiming at this problem, we propose a simple scheme to eliminate phase ambiguity and analyze its performance.

Methods A binary-outcome photon counting and joint likelihood function measurement are employed in this work, where the detection event with an equal number of photons is a measurement outcome. All the other detection events are treated as another outcome. We generalize it to a multi-output scenario and use single-photon states for joint measurement. According to the relationship between the maximum likelihood estimator and the inverse function estimator in the case of multiple outputs, we have semi-analytically explained the reason why this method works. Using the Monte Carlo method, we simulate the measurement probabilities of the six-photon twin-Fock state and the single-photon state and get a numerical simulation of the measurement scheme, where the experimental imperfection is added artificially.

Results and Discussions A strategy is proposed to eliminate the phase ambiguity of the twin-Fock state. Numerical simulation results verify that the strategy can eliminate phase ambiguity, and the phase sensitivity of the fluctuation of the estimator is better than the standard quantum limit in the whole phase interval. The main work is as follows: firstly, based on the related literature, the numerical simulation of the coincidence count measurement of the twin-Fock state light source and the single-photon light source in the Mach-Zehnder interferometer is carried out. Then the measurement strategy proposed in this paper is simulated, and the effectiveness of the simulation results is analyzed. Finally, the reduction sensitivity of the measurement strategy is given, and the whole phase interval is sampled to obtain statistical data. Furthermore, the unbiasedness of the estimator is verified numerically. The standard deviation of the measurement is compared with the theoretical expectation, the standard quantum limit, and the Heisenberg limit. The maximum likelihood estimation of the multi-output method for the twin-Fock state without bias phase was previously available, and it can be found that its likelihood function has two maximum points in a phase period. In this paper, we propose that when using multi-output measurement and maximum likelihood estimation, there is only one maximum point in a phase period if we combine the measurement results with the bias phase and without the bias phase to obtain the joint likelihood function. This paper gives an analysis of this phenomenon based on the approximation of linear combination estimators of maximum likelihood estimators. By generalizing the joint likelihood function measurement method of binary-outcome measurements to the multiple-output case, we find that it is possible to reduce the phase estimator from 4 to 2 in using only the twin-Fock state. Through the relationship between the maximum likelihood estimator and the inverse function estimator in the case of multiple outputs [Eqs. (9)-(14)], we have semi-analytically explained the reason why this method works. We then use the single-photon state for joint measurement, which ultimately eliminates phase ambiguity. Using the Monte Carlo method, we simulate the measurement process, and the results have validated our analysis results (Fig. 3). Finally, we calculate the Fisher information and the Cramer-Rao lower bound (CRB) of our measurement scheme as the analytical analysis of phase sensitivity. The numerical simulation results (Fig. 4) show that our estimator can beat the standard quantum limit.

Conclusions We propose a simple scheme to eliminate phase ambiguity of coincidence count detection for the twin-Fock

state. Our scheme relies on a sequence of the N -photons Fock states and the single-photon state that are injected into the interferometer to realize a single-peak structure of the total phase distribution, which determines the maximum likelihood estimator. Phase uncertainty of the estimator can beat the standard quantum limit over the entire phase interval.

Key words measurement; quantum metrology; twin-Fock state; phase ambiguity; maximum likelihood estimation